Quantum Annealing-Inspired Optimization for Space—Time Coding Metasurface

Shuai S. A. Yuan[®], Graduate Student Member, IEEE, Yutong Jiang[®], Graduate Student Member, IEEE, Ziyi Zhang, Student Member, IEEE, Jia Nan Zhang[®], Member, IEEE, Feng Liu[®], Jian Wei You[®], Senior Member, IEEE, and Wei E. I. Sha[®], Senior Member, IEEE

Abstract-Space-time coding metasurfaces introduce a new degree of freedom (DOF) in the temporal domain, enabling advanced manipulation of electromagnetic (EM) waves, particularly in controlling waves at different harmonic frequencies. Many applications of such metasurfaces rely on optimization algorithms to achieve specific functionalities. However, the computational cost of these algorithms becomes prohibitive when optimizing metasurfaces with large spatial and time dimensions. To address this challenge, we propose a quantum annealinginspired optimization framework designed to efficiently optimize space-time coding metasurfaces. First, the scattering behavior of space-time coding metasurface is mapped into the form of a binary spin model, where the phase of each meta-atom, including the discretization into arbitrary bits, is encoded as spins. Next, we construct the fitness function tailored to the desired optimization goals, and the resulting binary spin problem is then solved using a quantum-inspired simulated bifurcation (SB) algorithm. Finally, we demonstrate the effectiveness of our approach through several representative examples, including single-beam steering, multibeam steering, and waveform design at arbitrary harmonic frequencies. The proposed method significantly enhances the optimization efficiency, delivering high-quality solutions while substantially reducing computational time compared to genetic algorithms (GAs), quantum-inspired GAs (QGAs), and simulated annealing (SA). This advancement enables the practical optimization of large-scale space-time coding metasurfaces, paving the way for their broader application in advanced EM wave manipulation.

Index Terms—Beamforming, quantum-inspired optimization, simulated bifurcation, space–time coding metasurface.

I. INTRODUCTION

ETASURFACES, composed of subwavelength unit elements, have revolutionized the control of electromagnetic (EM) waves by enabling precise manipulation of amplitude, phase, and polarization [1]. These versatile structures can introduce phase differences at the subwavelength scale, facilitating numerous applications such as beamforming,

Received 17 January 2025; revised 30 April 2025; accepted 15 May 2025. Date of publication 2 June 2025; date of current version 8 September 2025. This work was supported by the National Natural Science Foundation of China under Grant 62401132, Grant 61975177, and Grant U20A20164. (Corresponding author: Wei E. I. Sha.)

Shuai S. A. Yuan, Yutong Jiang, Feng Liu, and Wei E. I. Sha are with the College of Information Science and Electronic Engineering, Zhejiang University, Hangzhou 310027, China (e-mail: weisha@zju.edu.cn).

Ziyi Zhang, Jia Nan Zhang, and Jian Wei You are with the State Key Laboratory of Millimeter Waves, School of Information Science and Engineering, Southeast University, Nanjing 210096, China.

Digital Object Identifier 10.1109/TAP.2025.3573526

filtering, and wavefront shaping [1]. The integration of both passive and active metasurfaces has demonstrated significant potential in advancing next-generation wireless communications [2]. Recently, time-modulated systems have garnered considerable attention for their ability to overcome existing limitations and enable unprecedented wave manipulation [3], [4], [5], [6]. In particular, recent developments in metasurfaces have introduced the concept of space–time coding, or time-modulated metasurfaces, which expand the capabilities of conventional metasurfaces through temporal modulation [7], [8], [9], [10], [11]. This additional degree of freedom (DOF), inspired by time-modulated antenna arrays [12], [13], [14], opens up unprecedented opportunities for dynamic and frequency-agile EM wave manipulation [15], [16], [17], [18].

Many designs of space-time coding metasurfaces rely on optimization algorithms to achieve specific functionalities [7], [8], [9], [10], [11], [15], [16]. As a discrete combinatorial optimization problem, the optimization of space-time coding metasurfaces poses significant challenges for traditional approaches such as genetic algorithms (GAs) and simulated annealing (SA). The inclusion of a time dimension exponentially increases the computational complexity, rendering the optimization process prohibitively slow. Alternative approaches, such as retrieving equivalent amplitude and phase [10], machine learning-based techniques [19], and space–time coding sequence optimization [9], have shown potential in addressing large-scale problems. However, these methods often involve extensive preprocessing, which is inherently time-consuming and typically requires further integration with optimization algorithms to achieve complex functionalities. As a result, achieving end-to-end optimizations under such constraints remains a substantial challenge in practical applications. This underscores the urgent need for the development of fast optimization approaches, or even real-time optimization techniques, to support the applications of space-time coding metasurfaces.

To tackle these challenges, we propose using the simulated bifurcation (SB) technique, a quantum annealing-inspired algorithm rooted in quantum physics. This method has proven to be significantly more effective than traditional algorithms in solving complex combinatorial optimization problems [20], [21], [22], [23]. Recent advancements in quantum electromagnetics and optimization techniques [24], [25], [26], [27] encompass areas such as quantum electrodynamics (QED)

simulations [28], [29], [30], quantum annealing-type algorithms [22], [23], [31], [32], [33], [34], quantum-inspired GAs (QGAs) [35], [36], and algorithms based on quantum circuits, such as variational quantum algorithms (VQAs) [37], [38] and quantum linear algebra [39], [40], all of which demonstrate substantial potential for a wide range of applications. Quantum annealing-type algorithms, in particular, have been investigated for practical beamforming problems in multi-input multi-output (MIMO) systems and metasurfaces [22], [23], [32], as well as for solving complex optimization problems in physics [24], [41] and wireless communications [42], [43]. Unlike quantum annealing executed on a quantum machine, which is constrained by the limited scale of problems due to the physical limitations of quantum components [25], quantum annealing-inspired optimization methods, such as the SB algorithm [20], [21], operate on classical computers. These methods offer significant advantages, including suitability for large-scale problems and parallel acceleration. Although it is a classical algorithm, it partially simulates the behavior of quantum systems and demonstrates performance comparable to algorithms executed on quantum machines for certain problems. However, the application of this method to the optimization challenges associated with space-time coding metasurfaces remains relatively underexplored, especially in key areas such as problem mapping, fitness function design, and validation through practical case studies.

This work introduces a novel quantum annealing-inspired algorithm tailored for the optimization of space-time coding metasurfaces. The key contributions of this research are as follows.

- Reformulating the scattering problem of space-time coding metasurfaces into a binary spin model. In this mapping, arbitrarily discretized phase states are encoded as spins, while spin-spin interactions capture the space-time synthesis of the metasurface elements.
- 2) Developing fitness functions tailored to desired scattering patterns, which enables arbitrary angular spectrum control at harmonic frequencies. These functions encapsulate the specific optimization objectives and are efficiently solved using the accelerated quantum-inspired SB solver. Comparisons with GA, QGA, and SA highlight the advantages of the proposed method.
- 3) Presenting several representative numerical examples, including single-beam steering, multibeam steering, and waveform design at arbitrary harmonic frequencies. These examples demonstrate the feasibility and efficiency of the proposed method.

The proposed approach overcomes the limitations of traditional methods by providing high-quality solutions with significantly reduced computational effort. This advancement not only enables rapid beam manipulation for space—time coding metasurfaces but also broadens their applicability in dynamic communication systems. Furthermore, the methodology can serve as an inspiration for applying quantum-inspired annealing techniques to a wider range of time-varying electromagnetic problems, including time-modulated antenna arrays and photonic time crystals.

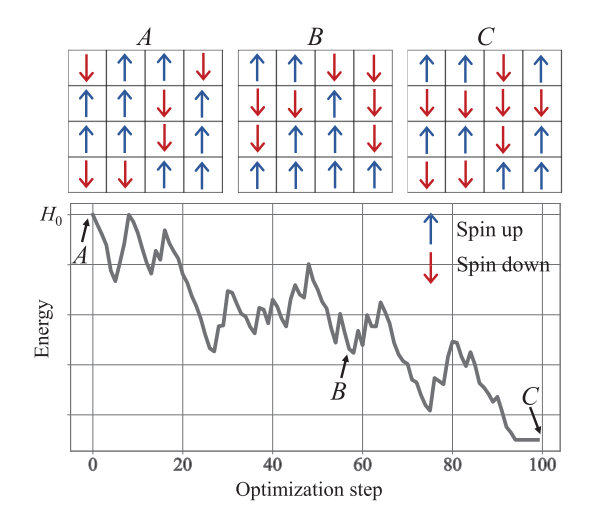


Fig. 1. Energy function, i.e., Hamiltonian, of the binary spin model varies throughout the optimization process, transitioning from an initial spin configuration (A) to a local minimum (B), and ultimately to the global minimum (C).

The remainder of this article is organized as follows: Section II introduces the principles of the proposed method, including the binary spin model, the mapping from the scattering of space–time coding metasurface to binary spin model, and the fitness function construction. Section III details the quantum-inspired SB algorithm for solving binary spin model, and evaluates its performance. Section IV showcases several representative applications of the space–time coding metasurface using the proposed method, such as beam steering and waveform design. Finally, Section V concludes this article with a summary and implications.

II. PRINCIPLES

A. Binary Spin Model

The binary spin model, inspired by the Ising model which was originally developed in statistical mechanics to describe ferromagnetism in materials [44], has found extensive applications in combinatorial optimization problems. The binary spin model can be expressed as

$$H = -\sum_{i=1}^{N} \sum_{j=1}^{N} J_{ij} s_i s_j$$
 (1)

where s_i is the binary spins that represent the state of the system (spin up or spin down in Fig. 1), J_{ij} represents the coupling or interaction between spins s_i and s_j , H is the Hamiltonian, or energy function, of the system, and \mathcal{N} here denotes the total number of spins. The objective of solving a binary spin model is to minimize the Hamiltonian, which corresponds to finding the configuration of spins s_i that leads to the lowest (ground) energy state. This optimization can be formulated as a quadratic unconstrained binary optimization (QUBO) problem, where minimizing the Hamiltonian corresponds to solving combinatorial tasks (e.g., maximizing an objective function). For higher order unconstrained binary optimization (HUBO), a generalized higher order Hamiltonian extends the framework, enabling solutions to more complex optimization problems [45]. Since the binary spin model can

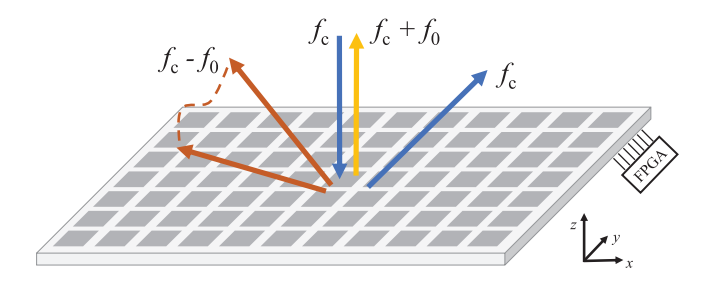


Fig. 2. Scattering of a space–time coding metasurface, controlled by an FPGA, allows the excitation of each meta-atom to vary over time, enabling precise control of waves at different harmonic frequencies.

be efficiently solved using quantum annealing machines or quantum-inspired algorithms, the beamforming problem can be reformulated into this model for rapid solutions, as first demonstrated in [32] and [34]. This process involves mapping the variables (phases) to spin states and carefully designing the objective function.

An intuitive example is provided in Fig. 1, showing the evolution of energy, i.e., Hamiltonian, during the optimization process. Spin configurations A, B, and C represent the states of the spins at the beginning, middle, and end of the optimization, respectively. Starting with H_0 and configuration A, a local optimum corresponding to configuration B is reached midway through the optimization. Ultimately, the best configuration, C, is achieved, yielding the lowest energy and representing the global optimal solution.

B. Scattering of Space-Time Coding Metasurface

For the scattering of a space–time coding metasurface controlled by a field-programmable gate array (FPGA), the excitation of each meta-atom varies over time, enabling beam control at different harmonic frequencies, as indicated by the Fourier transform [8]. For instance, as illustrated in Fig. 2, with a perpendicularly incident wave at central frequency f_c , it is possible to generate an anomalously reflected wave at f_c , a perpendicularly reflected wave at harmonic frequency $f_c + f_0$, and even a complex waveform at harmonic frequency $f_c - f_0$.

Without loss of generality, under the perpendicular incidence of a plane wave with a time-harmonic dependence $e^{j2\pi f_c t}$, the time-dependent scattering pattern of a xOy-plane placed space–time coding metasurface can be expressed as [8]

$$f(\theta, \varphi, t) = \sum_{n=1}^{N} \sum_{m=1}^{M} E_{mn}(\theta, \varphi) \Gamma_{mn}(t) e^{j(k_x md + k_y nd)}$$
(2)

where $E_{mn}(\theta, \varphi)$ represents the far-field pattern of the (m, n)th element at the central frequency f_c , and j is the imaginary unit. The parameter d represents the element spacing along the x- and y-directions, k_x and k_y are the wave numbers along the x- and y-axes, and $\Gamma_{mn}(t)$ is the time-modulated reflection coefficient of the (m, n)th element. $\Gamma_{mn}(t)$ is assumed to be a periodic function of time and is defined over one period as a linear combination of shifted pulse functions

$$\Gamma_{mn}(t) = \sum_{l=1}^{L} \Gamma_{mn}^{l} U_{mn}^{l}(t)$$
(3)

where $U_{mn}^l(t)$ is a periodic pulse function with a modulation period T_0 . Within each period, $U_{mn}^l(t)$ is defined as

$$U_{mn}^{l}(t) = \begin{cases} 1, & (l-1)\tau \le t \le l\tau \\ 0, & \text{otherwise} \end{cases}$$
 (4)

Here, $\tau = T_0/L$ denotes the pulsewidth of $U^l_{mn}(t)$, where L is the length of the time-coding sequence, and Γ^l_{mn} represents the reflection coefficient of the (m,n)th coding element during the interval $[(l-1)\tau, l\tau]$ at the central frequency. By applying a Fourier transform to $U^l_{mn}(t)$, we obtain

$$U_{mn}^{l}(t) = \sum_{h=-\infty}^{\infty} c_{mn}^{hl} e^{j2\pi h f_0 t}$$

$$\tag{5}$$

where $f_0 = 1/T_0$, h is the index for harmonic frequency, and the coefficients c_{mn}^{hl} are given by

$$c_{mn}^{hl} = \frac{1}{T_0} \int_0^{T_0} U_{mn}^l(t) e^{-j2\pi h f_0 t} dt.$$
 (6)

Thus, the Fourier series coefficients a_{mn}^h of the periodic function $\Gamma_{mn}(t)$ can be written as

$$a_{mn}^{h} = \sum_{l=1}^{L} \Gamma_{mn}^{l} c_{mn}^{hl} = \sum_{l=1}^{L} \frac{\Gamma_{mn}^{l}}{T_{0}} \int_{(l-1)\tau}^{l\tau} e^{-j2\pi h f_{0}t} dt$$

$$= \sum_{l=1}^{L} \frac{\Gamma_{mn}^{l}}{L} \operatorname{sinc}\left(\frac{\pi h}{L}\right) \exp\left[\frac{-j\pi h (2l-1)}{L}\right]. \tag{7}$$

Finally, the far-field scattering field of the space-time coding metasurface at the hth harmonic frequency $f_c + hf_0$ is given by

$$F^{h}(\theta,\varphi) = \sum_{n=1}^{N} \sum_{m=1}^{M} \sum_{l=1}^{L} \Gamma_{mn}^{l} / L \operatorname{sinc}\left(\frac{\pi h}{L}\right) E_{mn}(\theta,\varphi)$$

$$\times e^{j[k_{x}md + k_{y}nd - \pi h(2l-1)/L]}. \tag{8}$$

In this work, the far-field scattering field of a single metaatom, $E_{mn}(\theta, \varphi)$, is assumed to have a cosine shape, similar to that of a dipole antenna with a reflecting board, and is denoted as $E(\theta, \varphi)$. In addition, pure phase modulation is considered for beamforming, i.e., $|\Gamma^l_{mn}| = 1$.

C. Mapping the Scattering Problem Into Binary Spin Model

To map the scattering of a space-time coding metasurface into the binary spin model, the power pattern must be considered. The power pattern of the reflected wave is given by

$$P^{h}(\theta,\varphi) = |E(\theta,\varphi)|^{2} \sum_{n=1}^{N} \sum_{m=1}^{M} \sum_{l=1}^{L} \sum_{v=1}^{N} \sum_{u=1}^{M} \sum_{i=1}^{L} \Gamma_{mn}^{l} \Gamma_{uv}^{i} / L^{2}$$

$$\times \operatorname{sinc}^{2} \left(\frac{\pi h}{L} \right) e^{j \left[k_{x} (m-n)d + k_{y} (u-v)d - 2\pi h(l-i)/L \right]}$$

$$= \sum_{n=1}^{N} \sum_{m=1}^{M} \sum_{l=1}^{L} \sum_{v=1}^{N} \sum_{u=1}^{M} \sum_{i=1}^{L} \Gamma_{mn}^{l} \Gamma_{uv}^{i} A_{mnuv}^{li}$$
(9)

where

$$A_{mnuv}^{li} = |E(\theta, \varphi)|^2 / L^2 \operatorname{sinc}^2 \left(\frac{\pi h}{L}\right) \times e^{j[k_x(m-n)d + k_y(u-v)d - 2\pi h(l-i)/L]}.$$
 (10)

For conciseness, the harmonic index h is not explicitly indicated on the symbol of A^{li}_{mnuv} here, but is embedded within its expression. Now, we can recognize that this formulation aligns with the structure of the binary spin model. The spin-spin interactions not only account for interactions between antennas at different spatial positions but also incorporate temporal dimensions, forming an equivalent $M \times N \times L$ array. More explicitly, as a comprehensive example, for power focusing at a specific angle (θ_0, φ_0) at harmonic frequency h and a basic 1-bit problem, we have

$$H_{BF} = -P^{h}(\theta_{0}, \varphi_{0}) = -\sum_{p=1}^{N_{s}} \sum_{q=1}^{N_{s}} \Gamma_{p} \Gamma_{q} A_{pq}^{h}$$

$$= -\sum_{p=1}^{N_{s}} \sum_{q=1}^{N_{s}} s_{p} s_{q} J_{pq}$$
(11)

where the N_s represents the equivalent total number of antennas, defined as $N_s = M \times N \times L$. The number of indices p and q is equal to the number of spins and can be transformed into the previous indices as p = (m-1)NL + (n-1)L + l and q = (u-1)NL + (v-1)L + i in this 1-bit case. Terms related to angles are embedded in k_x and k_y . The mapping for the 1-bit case is straightforward because Γ_p , which represents the phase of the meta-atom, directly corresponds to the spin-down or spin-up state s_p , with values of 1 or -1. Therefore, the J_{pq} in the binary spin model is simply equal to A_{pq}^h . The negative sign before $P^h(\theta_0, \varphi_0)$ indicates power maximization, while power minimization can be achieved similarly, as the binary spin model inherently seeks the minimum energy configuration.

D. Phase Coding Method for Arbitrary Bits

For higher bit problems, Γ'_{mn} is no longer limited to values of 1 or -1, making direct coding impractical. To address this, a coding matrix can be introduced to map the phases into spins [22]. In general, for each atom with $n_{\rm bit}$ bits, at least $n_{\rm bit}$ spins are required to describe its phase. Consequently, a total of $M \times N \times L \times n_{\rm bit}$ spins are needed to describe the scattering of an $n_{\rm bit}$ space—time coding metasurface.

For example, in a 2-bit problem, the phase of a single metaatom can take values from the set $\{-j, -1, j, 1\}$. To represent this, two spins are used to encode the phase of a single atom. The phase of the first atom can be denoted as $\Gamma_1 = c_1 s_1 +$ $c_2 s_{1+N_s}$, where $c_1 = ((1+j)/2)$ and $c_2 = ((1-j)/2)$. For a certain beamforming angle (θ_0, φ_0) , the Hamiltonian for 2-bit case becomes

$$H_{BF} = -P^{h}(\theta_{0}, \varphi_{0}) = -c_{1}c_{1}^{*} \sum_{p=1}^{N_{s}} \sum_{q=1}^{N_{s}} s_{p}s_{q}A_{pq}^{h}$$

$$-c_{1}c_{2}^{*} \sum_{p=N_{s}+1}^{2N_{s}} \sum_{q=1}^{N_{s}} s_{p}s_{q}A_{pq}^{h} - c_{2}c_{1}^{*} \sum_{p=1}^{N_{s}} \sum_{q=N_{s}+1}^{2N_{s}} s_{p}s_{q}A_{pq}^{h}$$

$$-c_{2}c_{2}^{*} \sum_{p=N_{s}+1}^{2N_{s}} \sum_{q=N_{s}+1}^{2N_{s}} s_{p}s_{q}A_{pq}^{h} = \sum_{p=1}^{2N_{s}} \sum_{q=1}^{2N_{s}} s_{p}s_{q}J_{pq} \quad (12)$$

where * is the conjugate operator. J_{pq} consists of four parts and can be written as

$$J_{pq} = c_{\alpha} c_{\beta}^* A_{pq}^h, \quad \alpha, \beta \in \{1, 2\}$$

$$p \in [(\alpha - 1)N_s + 1, \alpha N_s]$$

$$q \in [(\beta - 1)N_s + 1, \beta N_s]. \tag{13}$$

In total, there are $2N_s$ spins and $2N_s \times 2N_s$ spin-spin interactions J_{pq} in the 2-bit case. However, for higher bit cases, the mapping from phase to spin and the corresponding coefficients become less explicit, necessitating the use of advanced encoding techniques.

For arbitrary bits, the problem can be generalized using a matrix representation [22]. For example, in the 2-bit case, the encoding can be expressed as $\mathbf{Sc} = \mathbf{p}$, represented in the following matrix form:

$$\mathbf{S} = \begin{bmatrix} 1 & 1 \\ 1 & -1 \\ -1 & 1 \\ -1 & -1 \end{bmatrix}, \quad \mathbf{c} = \begin{bmatrix} c_1 \\ c_2 \end{bmatrix}, \quad \mathbf{p} = \begin{bmatrix} \frac{\pi}{2} \\ \frac{3\pi}{2} \\ \frac{2\pi}{2} \end{bmatrix}$$
(14)

where S is the coding matrix, c is the coding coefficient vector to be determined, and p represents the discretized phase. It can be observed that the lower half of S is simply the negative of its upper half, and similarly, the lower half of the p vector is also the negative of its upper half (in exponential form). Therefore, the matrix can be reduced to

$$\mathbf{S} = \begin{bmatrix} 1 & 1 \\ 1 & -1 \end{bmatrix}, \quad \mathbf{c} = \begin{bmatrix} c_1 \\ c_2 \end{bmatrix}, \quad \mathbf{p} = \begin{bmatrix} \frac{\pi}{2} \\ \frac{\pi}{2} \end{bmatrix}. \tag{15}$$

This approach ensures that S is a full-rank matrix, allowing c to be uniquely solved using matrix inversion. However, for higher bit cases, such as the 3-bit problem, S is not a full-rank matrix but a 4×3 matrix. To address this, it is necessary to add a fourth column to make S full-rank for solving c. For the 3-bit problem, we use the product of three spins to fill the fourth column. Thus, we have

where c_1, c_2, c_3 correspond to s_1, s_2, s_3 , and c_4 corresponds to $s_1s_2s_3$. The spin-spin interactions consist of 16 parts, with each part containing $N_s \times N_s$ terms. For first-order interactions (involving c_1, c_2, c_3), there are a total of 9 parts. For third-order interactions (involving combinations of c_1, c_2, c_3 with c_4), there are 6 parts. Finally, there is 1 part involving c_4 with itself. The detailed expression is given as

$$H_{BF} = \sum_{p=1}^{3N_s} \sum_{q=1}^{3N_s} J_{pq} s_p s_q + \sum_{p=1}^{N_s} \sum_{q=1}^{3N_s} J_{pq}^Q s_p \prod_{q'=3q}^{3q+2} s_{q'}$$

$$+ \sum_{q=1}^{3N_s} \sum_{p=1}^{N_s} J_{qp}^Q s_q \prod_{p'=3p}^{3p+2} s_{p'} + \sum_{p=1}^{N_s} \sum_{q=1}^{N_s} J_{pq}^S \prod_{p'=3p}^{3p+2} s_{p'} \prod_{q'=3q}^{3q+2} s_{q'}$$

$$(17)$$

where

$$J_{pq} = c_{\alpha} c_{\beta}^* A^h, \quad \alpha, \beta \in \{1, 2, 3\}$$

$$p \in [(\alpha - 1)N_s + 1, \alpha N_s], \quad q \in [(\beta - 1)N_s + 1, \beta N_s] \quad (18)$$

and

$$J_{pq}^{Q} = c_{\alpha}c_{4}^{*}A^{h}, \quad \alpha \in \{1, 2, 3\}, \ p \in [(\alpha - 1)N_{s} + 1, \alpha N_{s}]$$

$$J_{pq}^{S} = -|c_{4}|^{2}A^{h}.$$
 (19)

For an arbitrary $n_{\rm bit}$ bits, we aim to use $n_{\rm bit}$ spins to represent the phase of each meta-atom. To achieve this, the matrix **S** must be made full-rank by adding the product of $n_{\rm bit}$ spins as additional spins. For an $n_{\rm bit}$ problem, we need to fill $2^{n_{\rm bit}-1}-n_{\rm bit}$ columns. For example, in a 4-bit case, we need to fill 4 columns, and we can directly use the combination of three spins, which is $C_4^3=4$, making the matrix an 8×8 full-rank matrix. For a 5-bit case, we need to fill $2^4-5=11$ columns, so we require all three-spin combinations, four-spin combinations, and a five-spin combination, as $C_5^3+C_5^4+C_5^5=11$. Thus, for any number of bits, we can construct the phase encoding in this manner, and the high-order binary spin model can be solved using a corresponding order-reduction method [45].

E. Fitness Function Construction

Once the scattering at a single angle for arbitrary bits is mapped to the form of the binary spin model, any desired fitness function for far-field manipulation can be constructed using a simple angular integral. This approach enables the design of angular ranges with varying power intensities, such as strong scattering in certain directions and weak scattering in others, at arbitrary harmonic frequencies. More generally, this concept can be expressed as a solid angle integral for each harmonic function. To implement this, we just need to replace A^h in the previous equations with \hat{A}^h as shown below for harmonic h

$$\hat{A}^h = \sum_n w_n^h \left(\int_{\Omega_n^h} A^h d\Omega \right) \tag{20}$$

where Ω_n^h denotes the *n*th solid angle range with harmonic index *h*, and w_n^h is the corresponding weight. For all harmonic manipulation, we can replace A^h by

$$\hat{A} = \sum_{h} \hat{A}^{h} = \sum_{h} \sum_{n} w_{n}^{h} \left(\int_{\Omega_{n}^{h}} A^{h} d\Omega \right). \tag{21}$$

By assigning positive or negative signs to w_n , we can control whether beamforming or beam suppression occurs within the target angular range. The amplitude of w_n determines the extent of the effect. Thus, using this fitness function, we can manipulate the power pattern of any harmonic over any farfield angular range through the proposed method, depending on the desired objective.

It should be noted that weight tuning becomes increasingly critical for intricate problems, as the Hamiltonian can be highly sensitive to changes in spin configurations. This sensitivity—particularly evident in complex tasks—is linked to the susceptibility of the SB algorithm to errors, as discussed in

[41]. In this context, complex tasks primarily refer to advanced functionalities such as multibeam beamforming or sophisticated radiation pattern synthesis, where small variations in weights or configuration parameters can cause significant fluctuations in the objective function.

III. QUANTUM-INSPIRED OPTIMIZATION ALGORITHM A. SB Optimizer

For the binary spin problem, a novel quantum adiabatic optimization method [46] utilizing a network of Kerr-nonlinear parametric oscillators (KPOs) has recently been proposed [20], [21]. The quantum Hamiltonian in this approach is expressed as

$$H_{q}(t) = \hbar \sum_{i=1}^{N} \left[\frac{K}{2} \hat{a}_{i}^{\dagger 2} \hat{a}_{i}^{2} - \frac{p(t)}{2} \left(\hat{a}_{i}^{\dagger 2} + \hat{a}_{i}^{2} \right) + \Delta_{i} \hat{a}_{i}^{\dagger} \hat{a}_{i} \right] - \hbar \xi_{0} \sum_{i=1}^{N} \sum_{i=1}^{N} J_{i,j} \hat{a}_{i}^{\dagger} \hat{a}_{j}$$
(22)

where \hbar is the reduced Planck constant, \hat{a}_i^{\dagger} and \hat{a}_i are the creation and annihilation operators, respectively, for the ith oscillator, and † denotes the Hermitian operator. In this context: K is the positive Kerr coefficient, p(t) is the time-dependent parametric two-photon pumping amplitude, Δ_i is the positive detuning frequency between the resonance frequency of the ith oscillator and half the pumping frequency, and ξ_0 is a positive constant with the dimension of frequency. The term J_{ij} represents the spin-spin interaction obtained from antenna synthesis, as discussed earlier. Initially, the state of each KPO is set to the vacuum state, and the pumping amplitude p(t) is gradually increased from zero to a sufficiently large value. The constant ξ_0 is chosen to be sufficiently small so that the vacuum state serves as the ground state of the initial Hamiltonian. Through a quantum adiabatic bifurcation process, each KPO ultimately transitions into a coherent state with either a positive or negative amplitude. The sign of the final amplitude for the ith KPO determines the ith spin of the ground state of the binary spin model, as ensured by the quantum adiabatic theorem.

The corresponding classical Hamiltonian system is obtained through a classical approximation, where the expectation value of \hat{a}_i is expressed as a complex amplitude, $x_i + iy_i$ (with i representing the imaginary unit). In this framework, the real part x_i and the imaginary part y_i serve as a pair of canonical conjugate variables, analogous to position and momentum, for the ith KPO. The classical mechanical Hamiltonian, along with the equations of motion governing this system, can be expressed as

$$H_{c}(\mathbf{x}, \mathbf{y}, t)$$

$$= \sum_{i=1}^{N_{s}} \left[\frac{K}{4} \left(x_{i}^{2} + y_{i}^{2} \right)^{2} - \frac{p(t)}{2} \left(x_{i}^{2} - y_{i}^{2} \right) + \frac{\Delta_{i}}{2} \left(x_{i}^{2} + y_{i}^{2} \right) \right] + \frac{\xi_{0}}{2} H_{BF}$$
(23)

where $H_{\rm BF}$ is the designed Hamiltonian for beamforming problems. In order to realize a fast numerical solution, some

small values are discarded [20], [21], and the equation is simplified as

$$H_{SB}(\mathbf{x}, \mathbf{y}, t) = \sum_{i=1}^{N_s} \frac{\Delta}{2} y_i^2 + V(\mathbf{x}, t)$$

$$= \sum_{i=1}^{N_s} \frac{\Delta}{2} y_i^2 + \sum_{i=1}^{N_s} \left[\frac{K}{4} x_i^4 + \frac{\Delta - p(t)}{2} x_i^2 \right]$$

$$+ \frac{\xi_0}{2} H_{BF}. \tag{24}$$

According to the property of canonical conjugate variables, the time derivatives of x_i and y_i are

$$\dot{x}_i = \frac{\partial H_{\rm SB}}{\partial y_i} = \Delta y_i \tag{25}$$

$$\dot{y}_i = -\frac{\partial H_{\text{SB}}}{\partial x_i} = -\left[Kx_i^2 - p(t) + \Delta\right]x_i - \frac{\xi_0}{2}\frac{\partial H_{\text{BF}}}{\partial x_i}.$$
 (26)

It can be observed that x_i and y_i are separated, so we can solve the equation with a four-order Runge–Kutta method [47]. Defining

$$\mathbf{z}(t) = \left[x_i(t), y_i(t) \right]^T \tag{27}$$

and

$$f(t, \mathbf{z}) = \left[\Delta y_i, -\left(Kx_i^2 - p(t) + \Delta\right)x_i - \frac{\xi_0}{2} \frac{\partial H_{BF}}{\partial x_i} \right]^T$$
 (28)

then we can calculate the slopes and update the **z**. This algorithm is inherently suitable for parallel computing, allowing the optimum ξ_0 to be effectively found in single run [22].

Recent studies have demonstrated the potential for hardware acceleration of quantum-inspired algorithms, particularly the SB algorithm. In [21], the SB algorithm was successfully implemented on an FPGA, achieving substantial speedup compared to conventional CPU-based simulations. The inherent parallelism and deterministic dynamics of the SB method make it highly compatible with digital hardware platforms such as FPGAs and application-specific integrated circuits (ASICs), enabling fast and energy-efficient optimization. Building on this, we envision embedding the SB algorithm directly into the hardware of a space-time coding metasurface. By integrating the SB solver with the metasurface's real-time control circuitry, the system can autonomously evolve toward optimal beamforming solutions with minimal latency. Moreover, the proposed model for space-time coding metasurfaces is also compatible with quantum annealing machines [25] and optical Ising machines [48], offering additional platforms for accelerated optimization.

B. Performance Evaluation

To demonstrate the feasibility of the SB algorithm, we consider a typical application of space—time coding metasurface: beamforming at a specific frequency while simultaneously suppressing side lobes at that frequency and minimizing the energy at other harmonic frequencies. This requires increasing the energy at the beamforming angle $(-H_1)$, suppressing the energy of side lobes at the central frequency (H_2) , and suppressing the energy of all harmonic frequencies (H_3) . During the simulated quantum annealing process, we monitor the

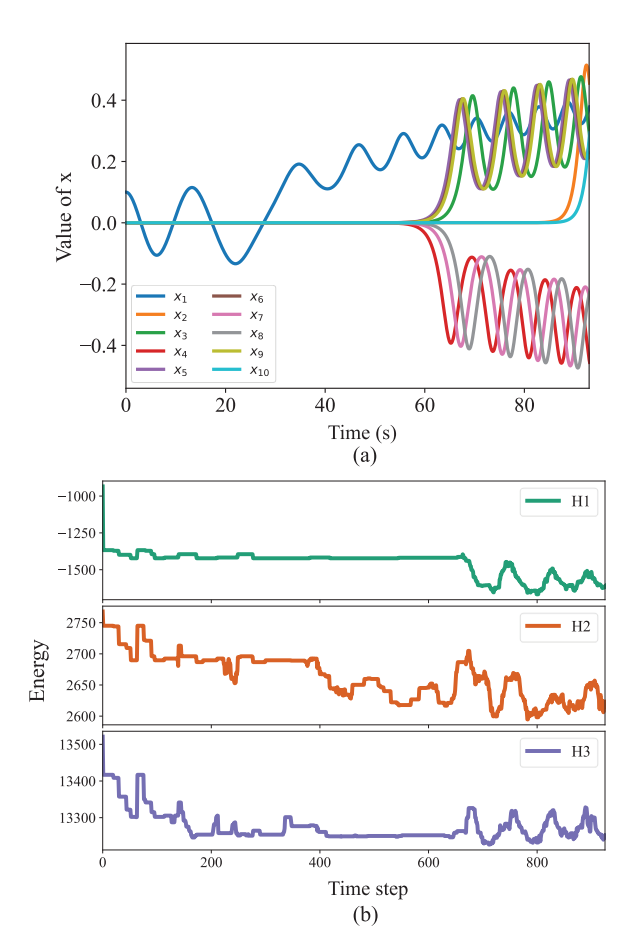


Fig. 3. Performance evaluation of the SB algorithm. (a) Bifurcation phenomenon observed during time evolution. (b) Decrease of energy across optimization steps, where $-H_1$, H_2 , and H_3 correspond to the beamforming energy at the central frequency, the sidelobe energy at the central frequency, and the energy of beams at all harmonic frequencies, respectively.

bifurcation phenomenon and the energy changes for these three components, as shown in Fig. 3. The bifurcation phenomenon is illustrated using the first ten spins in Fig. 3(a), demonstrating the algorithm's effectiveness. It can be observed that the energy of all three components gradually decreases in Fig. 3(b), indicating successful beamforming at the target angle and target frequency while suppressing energy elsewhere. It should be noted that the x values and the corresponding energy may appear to fluctuate, giving the impression that the optimization has not converged. However, only the sign of x is used to determine the final spin state—positive values correspond to "spin-up" (+1), and negative values to "spin-down" (-1). The algorithm is considered to have effectively converged once a bifurcation occurs in the x values, at which point each variable has clearly committed to a binary state. Therefore, the optimization can be safely terminated upon detecting this bifurcation, enabling faster computation without compromising accuracy.

We then evaluate the SB algorithm in comparison with GA, QGA, and SA. Specifically, we consider the standard 10×24 2-bit array beamforming problem with upper sidelobe suppression [22], which typically serves as a benchmark case for assessing optimization algorithm performance. To characterize and compare the efficiency of the algorithms, we adopt two metrics: single-run time and time-to-target (TTT)

TABLE I

COMPARISON OF OPTIMIZATION ALGORITHMS

Metric	SB	GA	QGA	SA
Time-to-Target (s)	15	60,904	50,063	3,275
Single-Run Time (s)	15	662	653	91

[49]. The TTT here is defined as

$$T = \frac{\ln\left(1 - P_d\right)}{\ln\left(1 - P_s\right)} \times t \tag{29}$$

where P_d is the desired success probability (set as 0.99), P_s is the success probability of finding a target solution in a single run, and t is the time for a single run. This metric captures the practical efficiency of an algorithm: even if a single run is fast, the TTT can still be large if the algorithm fails to reliably reach the target. Therefore, reporting both single-run time and TTT provides a more comprehensive benchmark for algorithm performance. In this study, the target solution is set as achieving at a 2.5 dB suppression in the upper sidelobe level (SLL) compared to the result obtained using only conventional beamforming phases.

The comparative results are summarized in Table I. As observed, the SB algorithm achieves nearly 40× faster singlerun execution compared to GA and QGA, and approximately 6× faster than SA. More importantly, SB consistently reaches the target solution in a single run with $T \approx t$, whereas GA, QGA, and SA exhibit significantly lower success rates. As a result, when evaluated in terms of TTT, SB demonstrates a remarkable advantage—achieving speedups of approximately 4000× over GA, 3300× over QGA, and 200× over SA. In this setting, SA shows a higher success rate in locating the target solution compared to GA. However, it also exhibits greater performance variability, with a tendency to produce suboptimal results and larger variance across runs. QGA is a quantum-inspired algorithm that integrates principles such as qubit representation and superposition-like behavior into a classical GA framework [36]. It has shown performance improvements in small-scale problems involving fewer than 32 binary variables [35]. However, in the context of the beamforming problem considered here, which involves more than 480 binary variables, QGA performs similar to the traditional GA and offers only marginal improvements. These observations are expected to generalize to other beamforming problems of similar scale and structure.

To further evaluate the solving time and scalability of the proposed method, we analyze the relationship between the number of spins (i.e., determined by the metasurface size and bit resolution) and the required optimization time. Fig. 4(a) illustrates the solving time as a function of the spin count, providing a practical reference for estimating computational requirements across different problem scales. To quantify scalability, the data are analyzed on a log-log scale in Fig. 4(b), and a power-law model is fit to estimate the empirical computational complexity. The resulting fit is given by $2.26 \times 10^{-4} \mathcal{N}^{1.82}$, where \mathcal{N} denotes the number of binary spins. The fit exponent of 1.82, which is close to quadratic scaling, indicates polynomial growth in complexity, demonstrating favorable computational scalability of the SB

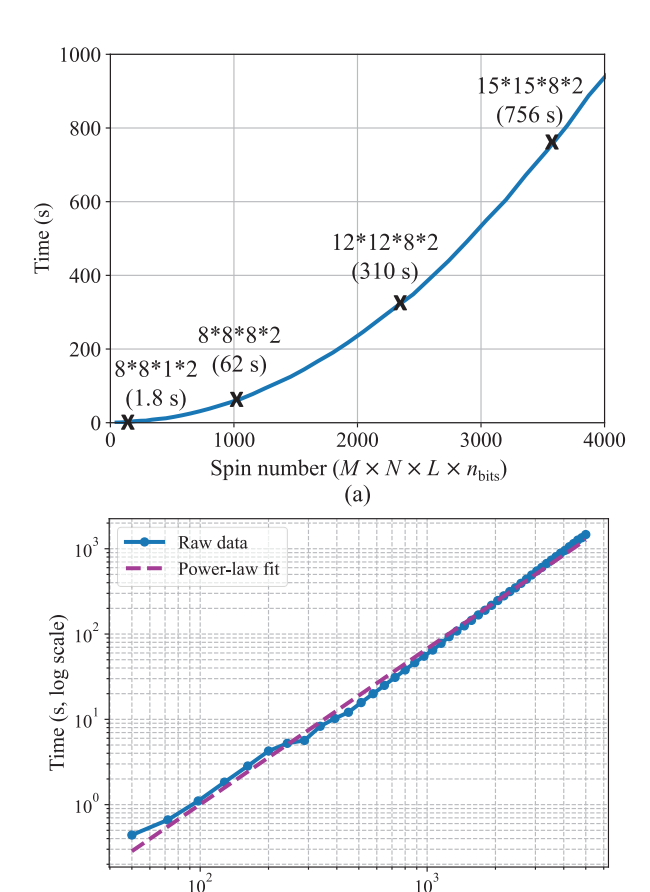


Fig. 4. Solving time of the binary spin model using SB algorithm. M, N, L, and n_{bits} denote the antenna number along x-direction, antenna number along y-direction, number of time slots, and number of bits for phase discretization, respectively. (a) Time versus spin number. (b) Log-log scale of the same data, with a power-law fit applied to estimate the computational complexity.

Spin number $(M \times N \times L \times n_{\text{bits}}, \log \text{ scale})$

(b)

algorithm. This model provides a predictive tool for estimating the solving time in larger metasurface configurations. While the algorithm imposes no fundamental limit on problem size, practical constraints such as computation time and memory usage become increasingly relevant as the number of spin grows. To address these challenges, future work will explore GPU acceleration and parallel computing strategies, which hold promise for significantly reducing optimization time.

IV. NUMERICAL RESULTS

A. Single Beam Steering

Time modulation can be treated as an additional DOF for phase tuning, akin to higher bit discretization, offering significant advantages in sidelobe suppression for beam steering problems [10]. We provide two examples as a demonstration: one focusing on beam steering at the central frequency and the other at a harmonic frequency.

1) Beam Steering at Central Frequency: In this scenario, our objective is to steer the beam toward a specific angle at the central frequency, while suppressing side lobes at the central frequency and minimizing energy at all other harmonic frequencies. As previously discussed, the fitness function incorporates three weighted components corresponding to beamforming, sidelobe suppression, and harmonic

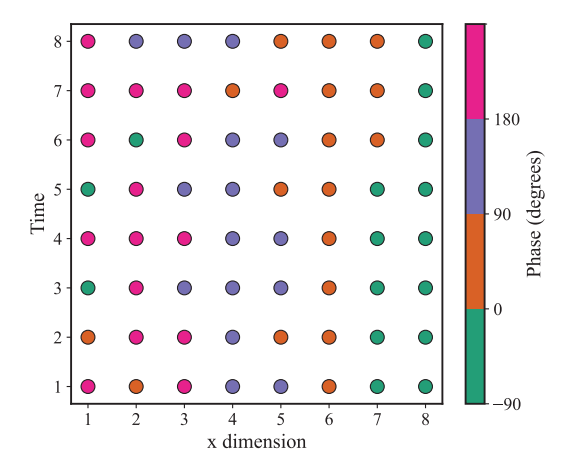


Fig. 5. Optimized excitation phases for the 2-bit $8 \times 8 \times 8$ space–time coding metasurface, which are designed to achieve single beam steering at $\theta = -14.5^{\circ}$ at the central frequency.

energy suppression. For beamforming at the central frequency, we assign a weight $w_1^0 = 10$ (the 1st angular range at the frequency order 0) and define the corresponding angular range as $\Omega_1^0 = \{-17^\circ < \theta < -12^\circ\}$. For sidelobe suppression at the central frequency, we set $w_2^0 = -0.4$ and define the angular range as $\Omega_2^0 = \{-90^\circ < \theta < 90^\circ\} \setminus \Omega_1^0$, operator \ denotes excluding the beamforming region Ω_1^0 . To suppress energy at all harmonic frequencies other than the central frequency, we assign weights $w_3^h = -0.3$ and define the angular range as $\Omega_3^h = \{-90^\circ < \theta < 90^\circ\}$, where $h \in \{-3, -2, -1, 1, 2, 3\}$ (i.e., $h \neq 0$).

Here, we consider a 2-bit $8\times8\times8$ space–time coding metasurface with translation invariance along the y-dimension as a benchmark, the same as the configuration in [8]. This reduces the total number of binary variables to $1\times8\times8\times2$. The optimized phases of the elements at different time slots are depicted in Fig. 5, while the optimized patterns at different harmonic frequencies are shown in Fig. 6(a). The results clearly demonstrate the effectiveness of the optimization, exhibiting SLL smaller than -14 dB and low sideband energy. A comparison between the far-field patterns with and without time modulation in Fig. 6(b) highlights the benefits of incorporating time modulation, as the results with the time modulation feature lower side lobes due to the equivalent effect of higher bit discretization. In many cases, achieving higher bit discretization—such as 2-bit or 3-bit RIS—is necessary to meet performance targets. However, from a hardware perspective, this is quite challenging, as it would require a large number of p-i-n diodes to implement these higher bit configurations, thereby increasing the hardware complexity and cost. Although time modulation introduces some additional computational complexity, it ultimately offers a more practical and cost-effective solution, especially in scenarios where implementing high-bit RIS is prohibitively expensive.

Furthermore, a sensitivity analysis is conducted to investigate the impact of weighting parameters on optimization performance. The primary beamforming weight was fixed at $w_1^0 = 10$ to ensure a strong emphasis on the main objective. The secondary weights w_2^0 and w_3^h were varied systematically, and their effects on the SLL at the central frequency and the

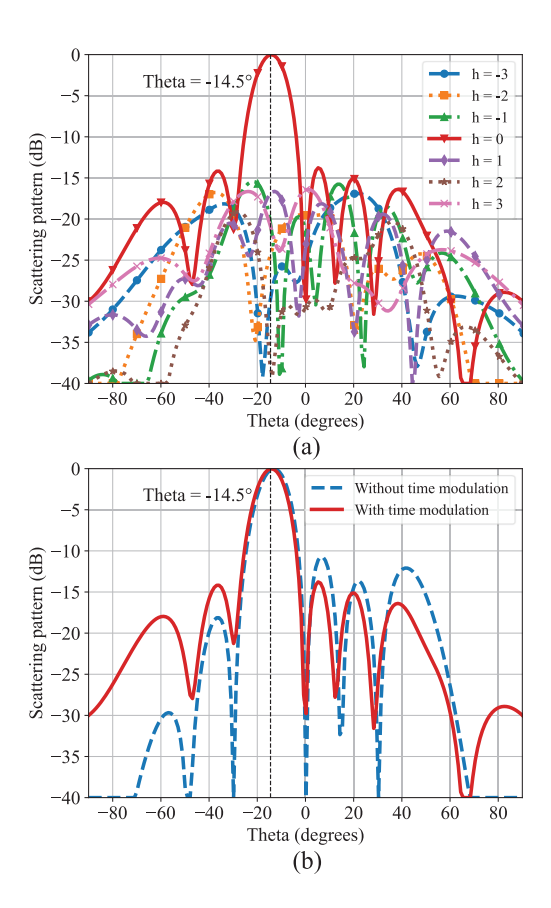


Fig. 6. Single beam steering pattern at the central frequency for the 2-bit $8\times8\times8$ space–time coding metasurface. (a) Central and harmonic far-field patterns. (b) Comparison between the far-field patterns with and without time modulation at central frequency.

maximum sideband lobe level were evaluated, as illustrated in Fig. 7. The results indicate that the optimization performance is jointly governed by w_2^0 and w_3^h . The SLL exhibits high sensitivity to w_2^0 , particularly when $w_3^h > 0.3$, whereas the maximum sideband lobe level is more sensitive when w_2^0 is large and w_3^h is small. This asymmetry highlights the importance of weight balancing in multiobjective formulations. To identify suitable weight combinations, a combination of empirical tuning and a dichotomous search strategy was employed. This hybrid approach leverages problem-specific insights while maintaining computational efficiency, as each optimization run completes rapidly. As a future direction, we plan to integrate automated weight selection methods—such as Bayesian meta-optimization or nested evolutionary strategies—to enable adaptive and task-aware tuning in real-time.

For this problem, another common approach is to retrieve the equivalent phase and amplitude of the meta-atoms [8], [10]. These methods are also very effective, but the process of searching for equivalent amplitude and phase could be time-consuming and often needs to be combined with optimization algorithms for complex tasks. In addition, this retrieval procedure may need to be repeated for each different array size, topology, and time sequence, further increasing the complexity. The proposed end-to-end optimization method can directly solve the beamforming problem and achieve comparable results, making it particularly advantageous for dynamic and large-scale problems.

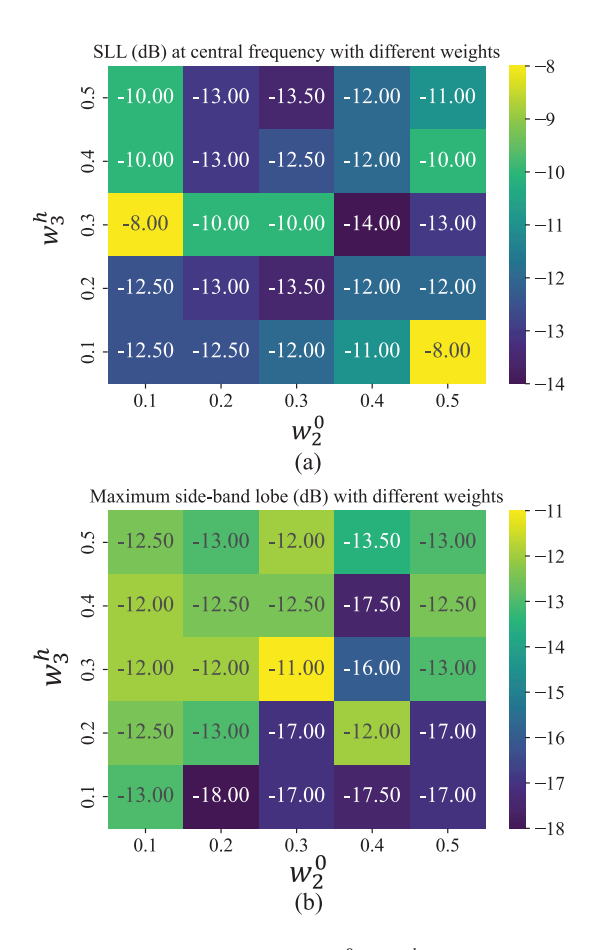


Fig. 7. Sensitivity analysis of the weights w_2^0 and w_3^h , where the beamforming weight w_1^0 is fixed as 10. (a) Effect of different weights on SLL at central frequency. (b) Effect of different weights on maximum sideband lobe.

2) Beam Steering at a Harmonic Frequency: Similar to beam steering at the central frequency, beam steering at an arbitrary harmonic frequency can also be achieved by modifying the fitness function. Still considering the same 2-bit $8 \times 8 \times 8$ space–time coding metasurface, we focus the beam at 28° for the harmonic frequency h = -1. We assign a weight θ < 30.5°}. For sidelobe suppression at h = -1, we set $w_2^{-1} = -0.3$ and define the angular range as $\Omega_2^{-1} = \{-90^{\circ} <$ $\theta < 90^{\circ} \setminus \Omega_1^{-1}$, excluding the beamforming region Ω_1^{-1} . To suppress energy at all harmonic frequencies other than h = -1, we assign weights $w_3^h = -0.2$ and define the angular range as $\Omega_3^h = \{-90^\circ < \theta < 90^\circ\}$, where $h \in \{-3, -2, 0, 1, 2, 3\}$. The optimized patterns at different harmonic frequencies are shown in Fig. 8(a). A comparison of beam patterns with and without time modulation is provided in Fig. 8(b), demonstrating good performance similar to beam steering at the central frequency.

B. Multiple Beam Steering

In addition to suppressing sideband beams and treating them as interference, it is also possible to harness them for beamforming—referred to as harmonic beamforming [14]. This enables the generation of beams in different directions, or in the same direction at different harmonic frequencies. In such scenarios, weight configurations from simpler cases, such

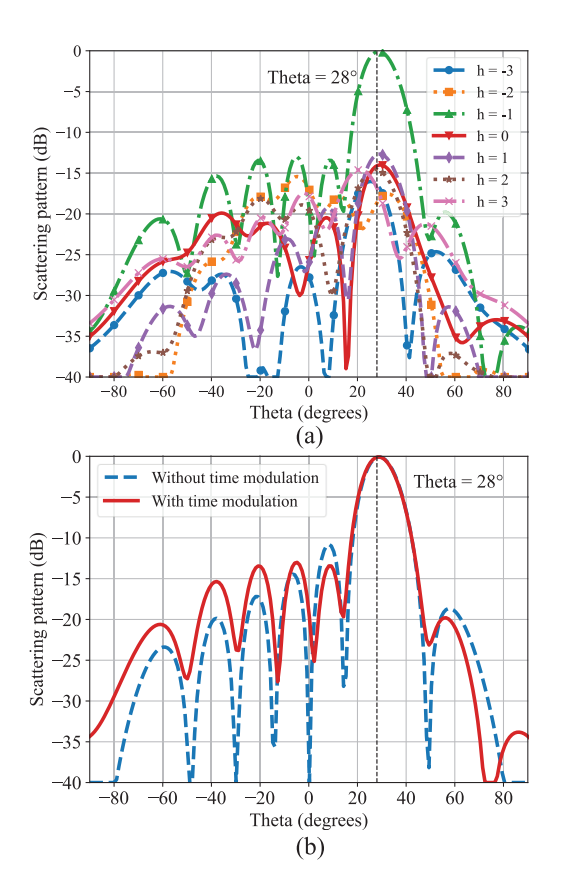


Fig. 8. Single beam steering pattern at the harmonic frequency h = -1 for the 2-bit $8 \times 8 \times 8$ space–time coding metasurface. (a) Central and harmonic far-field patterns. (b) Comparison between the far-field patterns with and without time modulation at harmonic frequency h = -1.

as the initial single-beam example, often serve as practical starting points for more complex tasks. This experience-driven strategy helps streamline the weight selection process. Several examples demonstrating these capabilities using the proposed method are presented below.

- 1) 2-Bit Beam Steering at Different Angles: In this scenario, we focus multiple beams along different directions corresponding to harmonic orders $h = \{-2, -1, 0, 1, 2\}$, with the beams directed at angles $\{-30^{\circ}, -15^{\circ}, 0^{\circ}, 15^{\circ}, 30^{\circ}\}$, respectively. Still using the 2-bit $8\times8\times8$ space–time coding metasurface, we assign weights $w_1^h = 10$ and define the angular range as $\Omega_1^h = \{-2.5^{\circ} + h \times 15^{\circ} < \theta < 2.5^{\circ} + h \times 15^{\circ}\}$, where $h \in \{-2, -1, 0, 1, 2\}$. The results, presented in Fig. 9(a), demonstrate good performance in harmonic beamforming at different angles.
- 2) 2-Bit Beam Steering at the Same Angle: Next, using the same metasurface configuration as above, we focus the beams at different harmonic frequencies along the same direction. For this case, we assign weights $w_1^h = 10$ and define the angular range as $\Omega_1^h = \{-2.5^\circ < \theta < 2.5^\circ\}$, where $h \in \{-2, -1, 0, 1, 2\}$. The results of harmonic beamforming at the same angle are depicted in Fig. 9(b), showing the wanted functionality.
- 3) 3-Bit Beam Steering at Different Angles: Then, we consider a 3-bit $8\times8\times8$ space—time coding metasurface, where the phases of all the meta-atoms can be tuned independently, resulting in a total of $3\times8\times8\times8$ binary variables. A

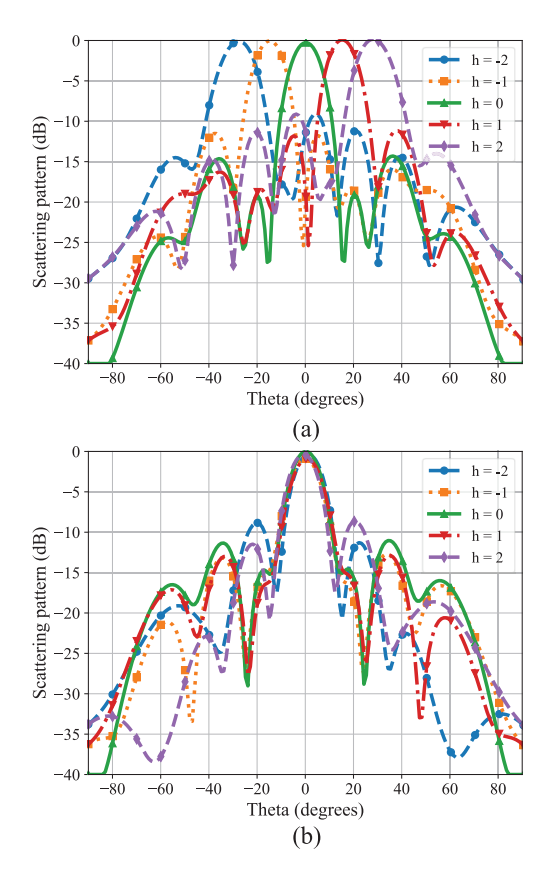


Fig. 9. Multiple beam steering patterns for the 2-bit $8 \times 8 \times 8$ space–time coding metasurface. (a) Generating steering beams along different directions at different frequencies. (b) Generating steering beams along the same direction at different frequencies.

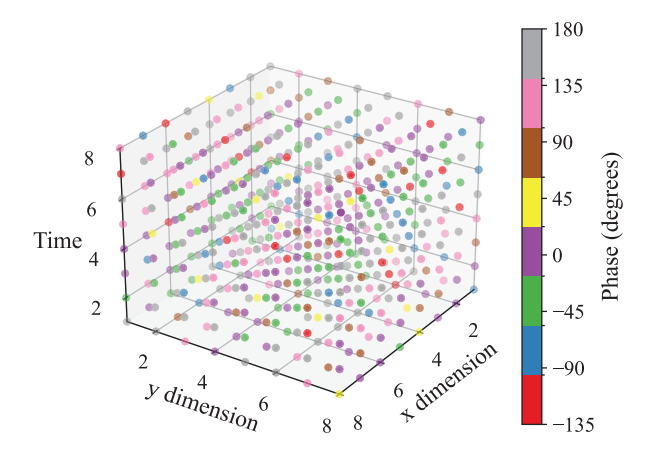


Fig. 10. Optimized excitation phases for the 3-bit $8 \times 8 \times 8$ space–time coding metasurface, which are designed to achieve beam steering at $(-30^{\circ}, 0^{\circ})$ when h = 1, and at $(0^{\circ}, 30^{\circ})$ when h = 2.

two-beam steering example is presented here, where the beam at the harmonic frequency h=1 is focused at $(-30^\circ,0^\circ)$, and the beam at the harmonic frequency h=2 is focused at $(0^\circ,30^\circ)$. For this case, we assign weights $w_1^1=10$ and $\Omega_1^2=\{-32.5^\circ<\theta<-27.5^\circ,-2.5^\circ<\varphi<2.5^\circ\}$, while $w_1^2=10$ and $\Omega_1^1=\{-2.5^\circ<\theta<2.5^\circ,27.5^\circ<\varphi<32.5^\circ\}$. The optimized excitation phases of the 3-bit space-time coding metasurface are shown in Fig. 10, varying across different

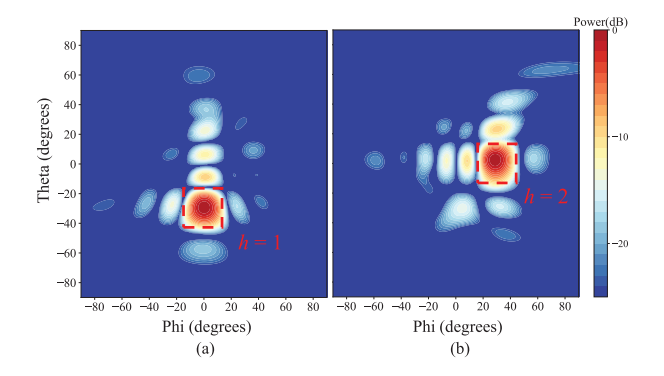


Fig. 11. 2-D multiple beam steering patterns for the 3-bit $8 \times 8 \times 8$ space—time coding metasurface. (a) Far-field pattern for h = 1. (b) Far-field pattern for h = 2.

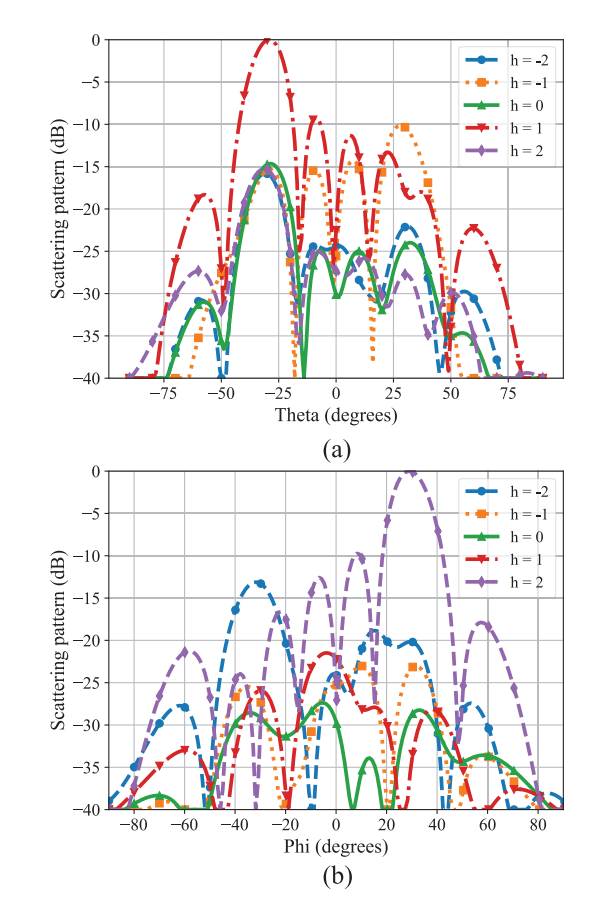


Fig. 12. 1-D multiple beam steering patterns at different frequencies for the 3-bit $8 \times 8 \times 8$ space—time coding metasurface. (a) Far-field pattern for h=1. (b) Far-field pattern for h=2.

positions and times. The corresponding 2-D and 1-D farfield scattering patterns at different frequencies are depicted in Figs. 11 and 12, respectively, demonstrating the effectiveness of the proposed method.

C. Waveform Design

Finally, we investigate the proposed method for waveform design using a space–time coding metasurface. Specifically, we design a square waveform for h = 2 and a beamforming pattern for h = -1. For this example, we use a 2-bit $15 \times 15 \times 8$ array, resulting in a total of 2×1800 binary variables for

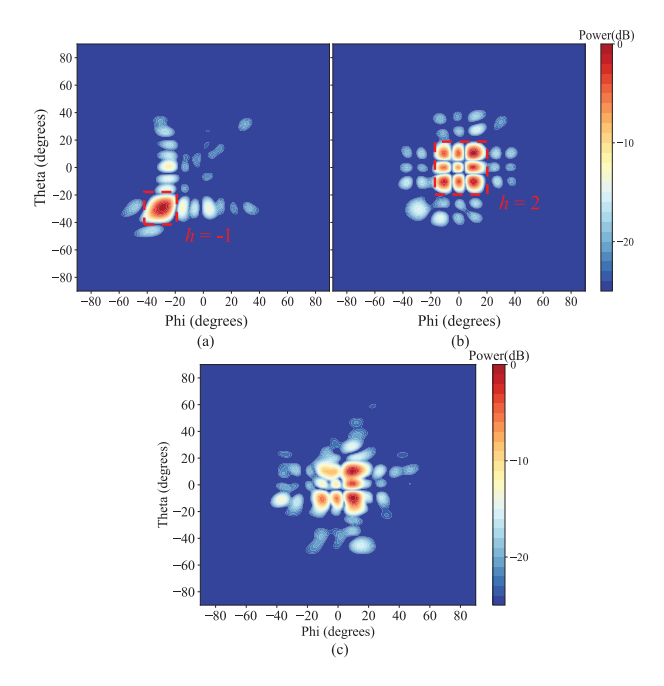


Fig. 13. 2-D waveform design patterns for the 2-bit $15 \times 15 \times 8$ space–time coding metasurface. (a) Pattern focusing at $(-30^{\circ}, -30^{\circ})$ for h = -1. (b) Pattern focusing within the area $\theta = -20^{\circ}$ to 20° and $\phi = -20^{\circ}$ to 20° for h = 2. (c) The square pattern is generated by a passive metasurface without time modulation.

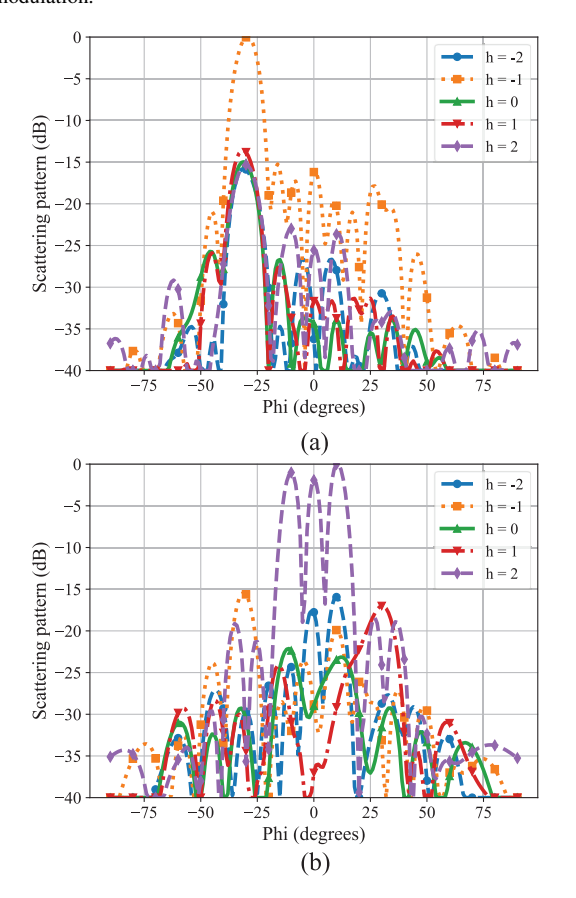


Fig. 14. 1-D waveform design patterns at different frequencies for the 2-bit $15\times15\times8$ space–time coding metasurface. (a) 1-D far-field pattern at $\theta=-30^\circ$. (b) 1-D far-field pattern at $\theta=-10^\circ$.

optimization. This scale of the problem presents significant challenges for algorithms such as GA, which typically require

substantial computational time. Moreover, generating a square waveform pattern cannot be directly achieved using certain analytical methods, as they often rely on continuous amplitude and phase control [50], which are not available in the considered discretized systems. For this case, we assign weights $w_1^{-1}=10$ and $\Omega_1^{-1}=\{-32.5^\circ < \theta < -27.5^\circ, -32.5^\circ < \varphi < -27.5^\circ\}$, while $w_1^2=8$ and $\Omega_1^2=\{-20^\circ < \theta < -27.5^\circ\}$ 20° , $-20^{\circ} < \varphi < 20^{\circ}$. As demonstrated in Fig. 13(a) and (b), high-quality beamforming and square waveform patterns are generated at h = -1 and h = 2, respectively. For comparison, the square beam pattern generated by a passive metasurface without time modulation is shown in Fig. 13(c), using the same objective function with the temporal modulation component disabled. As observed, the resulting pattern is more irregular and exhibits noticeable distortions even within the target angular range—unlike the more uniform and accurate pattern achieved when time modulation is applied. This demonstrates that, in the absence of time modulation, beam generation is not only restricted to the central frequency, but the overall beamforming performance also degrades due to insufficient discretizations. The 1-D waveform patterns at different frequencies at $\theta = -30^{\circ}$ and $\theta = -10^{\circ}$ are also plotted in Fig. 14, where the unwanted energy is suppressed, showcasing the effectiveness of the optimization algorithm. Penalty terms can be incorporated to further enhance the uniformity of the square pattern, achieving an approximation of a flattop pattern. This example demonstrates the flexibility of the proposed method and its ability to effectively tackle largescale, complex problems.

V. CONCLUSION

A quantum annealing-inspired algorithm is utilized to optimize space-time coding metasurfaces, effectively addressing the challenge of prolonged optimization times resulting from the increased number of variables introduced by the time dimension. The scattering behavior of the space-time coding metasurface is translated into a binary spin model, which is then optimized using an SB algorithm equipped with a carefully designed fitness function. The proposed optimization algorithm generally demonstrates strong performance across a range of beamforming targets, as shown in the presented examples. For more complex tasks, careful calibration of weights and penalty terms is essential. Future work will focus on further accelerating the algorithm, extending its application to more complex tasks such as upper sidelobe suppression, and conducting experimental validation using a fabricated space-time coding metasurface for real-time beamforming applications.

REFERENCE

- H.-T. Chen, A. J. Taylor, and N. Yu, "A review of metasurfaces: Physics and applications," *Rep. Prog. Phys.*, vol. 79, no. 7, Jul. 2016, Art. no. 076401.
- [2] M. Di Renzo et al., "Smart radio environments empowered by reconfigurable intelligent surfaces: How it works, state of research, and the road ahead," *IEEE J. Sel. Areas Commun.*, vol. 38, no. 11, pp. 2450–2525, Nov. 2020.
- [3] M. M. Asgari, P. Garg, X. Wang, M. S. Mirmoosa, C. Rockstuhl, and V. Asadchy, "Theory and applications of photonic time crystals: A tutorial," Adv. Opt. Photon., vol. 16, no. 4, p. 958, 2024.

- [4] H. Li, A. Mekawy, and A. Alú, "Beyond Chu's limit with floquet impedance matching," *Phys. Rev. Lett.*, vol. 123, no. 16, Oct. 2019, Art. no. 164102.
- [5] M. H. Mostafa, N. Ha-Van, P. Jayathurathnage, X. Wang, G. Ptitcyn, and S. A. Tretyakov, "Antenna bandwidth engineering through time-varying resistance," *Appl. Phys. Lett.*, vol. 122, no. 17, Apr. 2023, Art. no. 171703.
- [6] Z. Hayran and F. Monticone, "Using time-varying systems to challenge fundamental limitations in electromagnetics: Overview and summary of applications," *IEEE Antennas Propag. Mag.*, vol. 65, no. 4, pp. 29–38, Apr. 2023.
- [7] M. Nadi, A. Cheldavi, and S. Hassan Sedighy, "Beam steering toward multibeam radiation by time-coding metasurface antennas," *IEEE Trans. Antennas Propag.*, vol. 72, no. 6, pp. 4829–4838, Jun. 2024.
- Antennas Propag., vol. 72, no. 6, pp. 4829–4838, Jun. 2024.
 [8] L. Zhang et al., "Space-time-coding digital metasurfaces," Nature Commun., vol. 9, no. 1, p. 4334, Oct. 2018.
- [9] J. Y. Dai et al., "Arbitrary manipulations of dual harmonics and their wave behaviors based on space-time-coding digital metasurface," *Appl. Phys. Rev.*, vol. 7, no. 4, Dec. 2020, Art. no. 041408.
- [10] L. Zhang et al., "Dynamically realizing arbitrary multi-bit programmable phases using a 2-Bit time-domain coding metasurface," *IEEE Trans. Antennas Propag.*, vol. 68, no. 4, pp. 2984–2992, Apr. 2020.
- [11] X. Fang et al., "Accurate direction-of-arrival estimation method based on space-time modulated metasurface," *IEEE Trans. Antennas Propag.*, vol. 70, no. 11, pp. 10951–10964, Nov. 2022.
- [12] G. Li, S. Yang, Y. Chen, and Z.-P. Nie, "A novel electronic beam steering technique in time modulated antenna array," *Prog. Electromagn. Res.*, vol. 97, pp. 391–405, 2009.
- [13] H. Li, Y. Chen, and S. Yang, "Harmonic beamforming in antenna array with time-modulated amplitude-phase weighting technique," *IEEE Trans. Antennas Propag.*, vol. 67, no. 10, pp. 6461–6472, Oct. 2019.
- [14] L. Poli, P. Rocca, G. Oliveri, and A. Massa, "Harmonic beamforming in time-modulated linear arrays," *IEEE Trans. Antennas Propag.*, vol. 59, no. 7, pp. 2538–2545, Jul. 2011.
- [15] S. Taravati and G. V. Eleftheriades, "Microwave space-time-modulated metasurfaces," ACS Photon., vol. 9, no. 2, pp. 305–318, Jan. 2022.
- [16] D. Ramaccia, D. L. Sounas, A. Alú, A. Toscano, and F. Bilotti, "Phase-induced frequency conversion and Doppler effect with timemodulated metasurfaces," *IEEE Trans. Antennas Propag.*, vol. 68, no. 3, pp. 1607–1617, Mar. 2020.
- [17] S. A. Stewart, Tom. J. Smy, and S. Gupta, "Finite-difference time-domain modeling of space-time-modulated metasurfaces," *IEEE Trans. Antennas Propag.*, vol. 66, no. 1, pp. 281–292, Jan. 2018.
- [18] Z. Wu, C. Scarborough, and A. Grbic, "Space-time-modulated metasurfaces with spatial discretization: Free-space n -Path systems," *Phys. Rev. Appl.*, vol. 14, no. 6, Dec. 2020, Art. no. 064060.
- [19] M. Rossi et al., "Machine-learning-enabled multi-frequency synthesis of space-time-coding digital metasurfaces," Adv. Funct. Mater., vol. 34, no. 40, Oct. 2024, Art. no. 2403577.
- [20] H. Goto, K. Tatsumura, and A. R. Dixon, "Combinatorial optimization by simulating adiabatic bifurcations in nonlinear Hamiltonian systems," *Sci. Adv.*, vol. 5, no. 4, p. 2372, Apr. 2019.
- [21] H. Goto et al., "High-performance combinatorial optimization based on classical mechanics," *Sci. Adv.*, vol. 7, no. 6, p. 7953, Feb. 2021.
- [22] Y. Jiang et al., "Quantum-inspired beamforming optimization for quantized phase-only massive MIMO arrays," 2024, arXiv:2409.19938.
- [23] Q. J. Lim and Z. Peng, "Antenna array synthesis and optimization using simulated bifurcations of nonlinear oscillators," *Techrxiv*, Jul. 2024, doi: 10.36227/techrxiv.172175354.47227215/v1.
- [24] F. Hu et al., "Quantum computing cryptography: Finding cryptographic Boolean functions with quantum annealing by a 2000 qubit D-wave quantum computer," *Phys. Lett. A*, vol. 384, no. 10, Apr. 2020, Art. no. 126214.
- [25] N. Elsokkary, F. S. Khan, D. La Torre, T. Humble, and J. Gottlieb, "Financial portfolio management using D-wave quantum optimizer: The case of abu dhabi securities exchange," Oak Ridge Nat. Lab. (ORNL), Oak Ridge, TN, USA, Tech. Rep., 2017.
- Oak Ridge, TN, USA, Tech. Rep., 2017.

 [26] D. Pastorello and E. Blanzieri, "Quantum annealing learning search for solving QUBO problems," *Quantum Inf. Process.*, vol. 18, no. 10, p. 303, Oct. 2019.
- [27] M. D. Migliore, "Quantum computing for antennas and propagation problems: A gentle introduction," *IEEE Antennas Propag. Mag.*, vol. 67, no. 1, pp. 10–18, Feb. 2025.
- [28] W. E. I. Sha, A. Y. Liu, and W. C. Chew, "Dissipative quantum electromagnetics," *IEEE J. Multiscale Multiphys. Comput. Techn.*, vol. 3, pp. 198–213, 2018.

- [29] W. C. Chew, A. Y. Liu, C. Salazar-Lazaro, and W. E. I. Sha, "Quantum electromagnetics: A new Look—Part II," *IEEE J. Multiscale Multiphys. Comput. Techn.*, vol. 1, pp. 85–97, 2016.
- [30] T. E. Roth, R. Ma, and W. C. Chew, "The transmon qubit for electromagnetics engineers: An introduction," *IEEE Antennas Propag. Mag.*, vol. 65, no. 2, pp. 8–20, Apr. 2023.
- [31] S. Lee et al., "Quantum annealing for electromagnetic engineers—Part I: A computational method to solve various types of optimization problems," *IEEE Antennas Propag. Mag.*, early access, Dec. 13, 2024, doi: 10.1109/MAP.2024.3498695.
- [32] C. Ross, G. Gradoni, Q. J. Lim, and Z. Peng, "Engineering reflective metasurfaces with ising Hamiltonian and quantum annealing," *IEEE Trans. Antennas Propag.*, vol. 70, no. 4, pp. 2841–2854, Apr. 2022.
- [33] S. Lee, S. Han, W. Song, K.-J. Lee, and S. Kim, "Discrete source optimization for microwave hyperthermia using quantum annealing," *IEEE Antennas Wireless Propag. Lett.*, vol. 23, pp. 1095–1099, 2024
- [34] Q. J. Lim, C. Ross, A. Ghosh, F. W. Vook, G. Gradoni, and Z. Peng, "Quantum-assisted combinatorial optimization for reconfigurable intelligent surfaces in smart electromagnetic environments," *IEEE Trans. Antennas Propag.*, vol. 72, no. 1, pp. 147–159, Jan. 2024.
- [35] Z. Xu, W. Shang, S. Kim, A. Bobbitt, E. Lee, and T. Luo, "Quantum-inspired genetic algorithm for designing planar multilayer photonic structure," npj Comput. Mater., vol. 10, no. 1, p. 257, Nov. 2024.
- [36] R. Lahoz-Beltra, "Quantum genetic algorithms for computer scientists," Computers, vol. 5, no. 4, p. 24, Oct. 2016.
- [37] E. Colella, S. Beloin, L. Bastianelli, V. M. Primiani, F. Moglie, and G. Gradoni, "Variational quantum shot-based simulations for waveguide modes," *IEEE Trans. Microw. Theory Techn.*, vol. 72, no. 4, pp. 2084–2094, Apr. 2024.
- [38] E. Colella, L. Bastianelli, V. M. Primiani, Z. Peng, F. Moglie, and G. Gradoni, "Quantum optimization of reconfigurable intelligent surfaces for mitigating multipath fading in wireless networks," *IEEE J. Multiscale Multiphys. Comput. Techn.*, vol. 9, pp. 403–414, 2024.
- [39] L. Tosi, P. Rocca, N. Anselmi, and A. Massa, "Array-antenna power-pattern analysis through quantum computing," *IEEE Trans. Antennas Propag.*, vol. 71, no. 4, pp. 3251–3259, Apr. 2023.
- [40] J. Zhang, F. Feng, and Q.-J. Zhang, "Quantum computing method for solving electromagnetic problems based on the finite element method," *IEEE Trans. Microw. Theory Techn.*, vol. 72, no. 2, pp. 948–965, Feb. 2024.
- [41] Q.-G. Zeng, X.-P. Cui, B. Liu, Y. Wang, P. Mosharev, and M.-H. Yung, "Performance of quantum annealing inspired algorithms for combinatorial optimization problems," *Commun. Phys.*, vol. 7, no. 1, p. 249, Jul. 2024.
- [42] T. Q. Dinh, S. H. Dau, E. Lagunas, S. Chatzinotas, D. N. Nguyen, and D. T. Hoang, "Quantum annealing for complex optimization in satellite communication systems," *IEEE Internet Things J.*, vol. 12, no. 4, pp. 3771–3784, Feb. 2025.
- [43] M. Kim, D. Venturelli, and K. Jamieson, "Leveraging quantum annealing for large MIMO processing in centralized radio access networks," in *Proc. ACM Special Interest Group Data Commun.*, Aug. 2019, pp. 241–255.
- [44] T. D. Schultz, D. C. Mattis, and E. H. Lieb, "Two-dimensional ising model as a soluble problem of many fermions," *Rev. Modern Phys.*, vol. 36, no. 3, pp. 856–871, Jul. 1964.
- [45] B.-Y. Wang, X. Cui, Q. Zeng, Y. Zhan, M.-H. Yung, and Y. Shi, "Speedup of high-order unconstrained binary optimization using quantum Z2 lattice gauge theory," 2024, arXiv:2406.05958.
- [46] A. M. Childs, E. Farhi, and J. Preskill, "Robustness of adiabatic quantum computation," *Phys. Rev. A, Gen. Phys.*, vol. 65, no. 1, Dec. 2001, Art. no. 012322.
- [47] J. H. E. Cartwright and O. Piro, "The dynamics of Runge-Kutta methods," Int. J. Bifurc. Chaos, vol. 2, no. 3, pp. 427–449, Sep. 1992.
- [48] QBoson. (2025). Qboson Official Website. [Online]. Available: https:// www.qboson.com/
- [49] J. King, S. Yarkoni, M. M. Nevisi, J. P. Hilton, and C. C. McGeoch, "Benchmarking a quantum annealing processor with the time-to-target metric," 2015. arXiv:1508.05087.
- [50] A. Aghasi, H. Amindavar, E. L. Miller, and J. Rashed-Mohassel, "Flat-top footprint pattern synthesis through the design of arbitrary planar-shaped apertures," *IEEE Trans. Antennas Propag.*, vol. 58, no. 8, pp. 2539–2552, 2010.



Shuai S. A. Yuan (Graduate Student Member, IEEE) received the B.Eng. degree from Nanjing University of Aeronautics and Astronautics, Nanjing, China, in 2019, and the Ph.D. degree in electronic science and technology from Zhejiang University, Hangzhou, China, in 2024.

From March 2023 to March 2024, he was a Visiting Ph.D. Student at ELEDIA Research Center, University of Trento, Trento, Italy. His research interests include electromagnetic information theory, antenna and metasurface designs inspired by electro-

magnetic information theory, and quantum-inspired optimization.



Feng Liu received the bachelor's degree from Yantai University, Yantai, China, in 2008, the master's degree from the University of Sheffield, Sheffield, U.K., in 2019, and the Ph.D. degree from the Technical University Dortmund (TU Dortmund), Dortmund, Germany, in 2013.

He was a Post-Doctoral Researcher at the University of Sheffield and RWTH Aachen University, Aachen, Germany, from 2013 to 2019. In 2019, he joined the College of Information Science and Electronic Engineering, Zhejiang University,

Hangzhou, China, where he is currently a tenured Associate Professor. His research focuses on quantum light sources based on III-V quantum dots, cavity/waveguide-QED, and integrated quantum optical circuits.



Yutong Jiang (Graduate Student Member, IEEE) received the B.Sc. degree in electronic science and technology from Zhejiang University, Hangzhou, China, in 2023, where she is currently pursuing the M.Sc. degree in electronic science and technology.

Her research interests include antenna array optimization, machine learning, quantum-inspired algorithms, electromagnetic beamforming for MIMO, coupling modeling, and electromagnetic channel modeling.

Ms. Jiang was a recipient of the Best Student Paper Award (Top Prize) at IEEE ACES-China in 2024.



Jian Wei You (Senior Member, IEEE) received the B.Sc. degree in electrical engineering from Xidian University, Xi'an, China, in 2010, and the Ph.D. degree in electromagnetic field and microwave techniques from Southeast University, Nanjing, China, in 2016.

From 2016 to 2021, he was a Research Associate with the Department of Electronic and Electrical Engineering, University College London, London, U.K. In 2021, he joined Southeast University, as a Full Professor. His research interests include com-

putational electromagnetics, metamaterials, microwave and millimeter-wave devices, multiphysics and multiscale simulations, topological metasurfaces, and quantum information.



Ziyi Zhang (Student Member, IEEE) was born in Jiangsu, China, in 2003. He is currently pursuing the B.E. degree in electronic and information engineering from Sichuan University, Chengdu, China.

His research interests include programmable metasurfaces and applications of deep learning in microwave component design.



Jia Nan Zhang (Member, IEEE) received the B.Eng. degree from Tianjin University, Tianjin, China, in 2013, and the joint Ph.D. degree from the School of Microelectronics, Tianjin University, and the Department of Electronics, Carleton University, Ottawa, ON, Canada, in 2020.

From 2020 to 2022, he was a Post-Doctoral Research Associate with the Department of Electronics, Carleton University. In January 2022, he joined the State Key Laboratory of Millimeter Waves, Southeast University, Nanjing, China, where

he is currently a Professor. He has authored/co-authored over 80 publications in prestigious microwave journals/conferences. He contributed to the *Encyclopedia of Surrogate Modeling for High-Frequency Design: Recent Advances* (World Scientific, 2021) and the *Uncertainty Quantification of Electromagnetic Devices, Circuits, and Systems* (IET, 2021). His research interests include intelligent EM computation, machine-learning approaches to metasurface inverse design, and quantum computing with applications to EM problems.

Dr. Zhang is a member of the IEEE Microwave Theory and Techniques Society (IEEE MTT-S) and the IEEE Antennas and Propagation Society (IEEE AP-S). He served as the General Chair for the 2022 IEEE MTT-S Young Professionals Workshop on Electromagnetic Modeling and Optimization (EMO 2022). He is a reviewer of a number of renowned microwave journals, including IEEE TRANSACTIONS ON MICROWAVE THEORY AND TECHNIQUES, IEEE TRANSACTIONS ON CIRCUITS AND SYSTEMS I: REGULAR PAPERS, IEEE ANTENNAS AND WIRELESS PROPAGATION LETTERS, and IEEE MICROWAVE AND WIRELESS TECHNOLOGY LETTERS.



Wei E. I. Sha (Senior Member, IEEE) received the B.S. and Ph.D. degrees in electronic engineering from Anhui University, Hefei, China, in 2003 and 2008, respectively.

From July 2008 to July 2017, he was a Post-Doctoral Research Fellow and later a Research Assistant Professor with the Department of Electrical and Electronic Engineering, University of Hong Kong, Hong Kong. Between March 2018 and March 2019, he held a Marie Skłodowska-Curie Individual Fellowship at University College London,

London, U.K. In October 2017, he joined the College of Information Science and Electronic Engineering, Zhejiang University, Hangzhou, China, where he is currently a tenured Associate Professor. His research focuses on theoretical and computational electromagnetics, including computational and applied electromagnetics, nonlinear and quantum electromagnetics, micro- and nanooptics, and multiphysics modeling. He has authored or co-authored over 200 peer-reviewed journal articles, 180 conference papers, 12 book chapters, and two books. His work has been cited over 11700 times on Google Scholar, with an H-index of 58.

Dr. Sha is a Life Member of OSA. He received multiple awards, including the ACES-China Electromagnetics Education Ambassador Award in 2024, the ACES Technical Achievement Award in 2022, and the PIERS Young Scientist Award in 2021. Nine of his students have won Best Student Paper Awards. He has reviewed more than 60 technical journals and served on the Technical Program Committees of over ten IEEE conferences. He is an Associate Editor for IEEE JOURNAL ON MULTISCALE AND MULTIPHYSICS COMPUTATIONAL TECHNIQUES, IEEE OPEN JOURNAL OF ANTENNAS AND PROPAGATION, IEEE ACCESS, and *Electromagnetic Science*.